RESEARCH ARTICLE

Nephrocytes is a part of the spectrum of podocyte diversity

Takayuki Miyaki[1], Yuto Kawasaki[1], Akira Matsumoto[2], Soichiro Kakuta[3], Tatsuo Sakai[1], and Koichiro Ichimura[1, 3*]

[1] Department of Anatomy and Life Structure, Juntendo University Graduate School of Medicine, Tokyo, Japan;
[2] Department of Biology, Juntendo University School of Medicine, Inzai, Chiba, Japan;
[3] Laboratory of Morphology and Image Analysis, Center for Biomedical Research Resources, Juntendo University Graduate School of Medicine, Tokyo, Japan.

***Author for Correspondence**: Dr. Koichiro Ichimura, Department of Anatomy and Life Structure, Juntendo University Graduate School of Medicine, 2-1-1 Hongo, Bunkyo-ku, Tokyo 113-8421, Japan; E-mail: ichimura@juntendo.ac.jp

Running Title: 3D ultrastructure of decapod nephrocytes

Key Words: 3D ultrastructure, podocytes, nephrocytes, decapod, FIB-SEM tomography

ABSTRACT

The excretory system produces urine by ultrafiltration via a filtration epithelium. Podocytes are widely found in eucoelomates as the filtration epithelial cells. In some eucoelomates including insects and crustaceans, nephrocytes, which separate toxic substances from hemolymph, are found in addition to podocytes. *Drosophila* nephrocytes, which possess structural similarity to podocytes, have recently utilized as a model system to study podocyte function and disease. However, in actually, the functional property and cellular architecture are strikingly different between *Drosophila* nephrocytes and eucoelomate podocytes—the phylogenetic relation of these cells is enigmatic. In this study, using volume scanning electron microscopy, we found the decapod nephrocytes exhibited more highly structural similarity to podocytes than previously known in the *Drosophila* nephrocytes. The decapod nephrocytes filled a "*missing link*" in the evolution of nephrocytes and podocytes, we thus concluded the nephrocyte is a part of the spectrum of podocyte diversity in animal phylogeny.

INTRODUCTION

Excretion is crucial to maintain the homeostasis of body fluid in multicellular animals (Andrikou et al., 2019; Evans, 2008). Their excretory systems generally produces primary urine by ultrafiltration of body fluid via a filtration epithelium. The primary urine is subsequently transferred to a modulating tubule, where the final urine is produced from the primary urine by epithelial secretion and reabsorption (**Fig. S1a–d, a'–d'**) (Ichimura and Sakai, 2017; Ruppert et al., 2003).

Eucoelomate animals, which possess the coelom or coelomic sac laying the methothelium, alter a part of methothelium into the filtration epithelium composed by podocytes (Ruppert and Smith, 1988). The primary urine excluded into the coelomic lumen via the podocyte-based filtration epithelium and then enter into the nephridium, a kind of modulating tubule, which open to the coelomic cavity (**Fig. S1b, c**). In vertebrates, the Bowman's capsule, which contains the podocyte-based filtration epithelium, can be regarded as a micro-coelomic sac newly formed in the mesonephric and metanephric kidneys (Ichimura and Sakai, 2018; Ruppert, 1994) (**Fig. S1d, d'**).

Podocytes exhibit a characteristic architecture that is specialized for the ultrafiltration of body fluid (Ichimura et al., 2017; Ichimura et al., 2007; Ichimura et al., 2019; Ichimura et al., 2015; Kriz and Kaissling, 2007; Pavenstadt et al., 2003). In vertebrates, the voluminous cell body of a podocyte projects several thick primary processes (**Fig. S2**). From the cell body and primary processes, the ridge-like prominences (RLPs) are protruded to adhere themselves to the basement membrane. Furthermore, a number of fine foot processes are protruded via the RLPs. Adjacent podocytes are interdigitated with each other at their foot processes, which are separated from each other by filtration slits and bridged with a specialized intercellular junction, slit diaphragm, which serves as a part of filtration barrier apparatus (**Fig. 1a1–3**) (Assady et al., 2017; Ichimura et al., 2013; Ichimura et al., 2012).

Some groups of eucoelomate animals (Arthropoda, Onycophora, and Mollusca) possess nephrocytes, which are similar to podocytes in structure, in addition to podocytes (Crossley, 1984; Haszprunar, 1996; Seifert and Rosenberg, 1977). Nephrocytes and podocytes commonly exhibit numerous fine foot processes bridged by slit diaphragms—the molecular components of slit diaphragm are highly conserved between the nephrocytes in *Drosophila melanogaster* and podocytes in vertebrates

(Weavers et al., 2009; Zhuang et al., 2009). The researchers in the field of podocyte biology and nephrology have recently taken advantage of the similarities to use *Drosophila* nephrocytes as a model system to study podocyte function and disease (Fu et al., 2017; Helmstädter and Simons, 2017; Na et al., 2015; Tutor et al., 2014; Weide et al., 2017).

Although nephrocytes and podocytes exhibit the similarity in several aspects, the function and cellular architecture greatly differ between them (**Fig. 1**). Unlike podocytes, individual *Drosophila* nephrocytes are completely surrounded by basement membrane, thus they do not form an epithelial sheet and do not link to the Malpighian tubule, a modulating tubule peculiar to insets (**Figs. 1b1, S1e**). Therefore nephrocytes are not involved in the production of primary urine, but they serve to separate toxic substances, such as heavy metals, from hemolymph by endocytosis (Crossley, 1984). Moreover, the formation of foot processes differs greatly between *Drosophila* nephrocytes and vertebrate podocytes (Kawasaki et al., 2019). As mentioned above, the podocyte foot processes are formed by protrusion and are interdigitated between adjacent podocytes, and thus the podocyte slit diaphragm is an intercellular junction (**Fig. 1a1–3**). In contrast, the nephrocyte foot processes are formed by infolding/invagination of the basal plasma membrane in *Drosophila* since the nephrocytes exist as solitary cells, resulting that the nephrocyte slit diaphragm is an autocellular junction in this animal (**Fig. 1b1–3**).

For understanding the evolution of the nephrocytes, we have reevaluated the structural diversity of nephrocytes in various taxonomic groups using focused-ion beam-scanning electron microscopy (FIB-SEM) tomography, a kind of volume scanning electron microscopy (Heymann et al., 2006; Kubota, 2015; Ohno et al., 2015; Titze and Genoud, 2016). Through our studies, we found the decapod nephrocytes exhibited more highly structural similarity to podocytes than previously known in the *Drosophila* nephrocytes—they filled the enormous gap between the solitary nephrocytes in *Drosophila* and the epithelium-forming podocytes, which could be called a "*missing link*" in the evolutionary diversity of nephrocytes and podocytes. In the present study, we demonstrated the 3D architecture of decapod nephrocytes and discussed the nephrocyte is a part of the spectrum of podocyte diversity in animal phylogeny.

RESULTS

Living decapod crustaceans (Decapoda) are classified into two suborders, Dendorobrachiata and Pleocyemata. The latter suborder is further divided into nine infraorders (**Fig. S3**) (Tsang et al., 2008). In the present study, we evaluated the 3D architecture of nephrocytes in five species of decapod crustaceans from five different taxonomic groups (**Fig. S3**; **Table S1**) using FIB-SEM tomography. This technique enables the efficient acquisition of a series of sectional images directly from resin-embedded biological samples (Miyaki et al., 2020a, b; Ohta et al., 2012). The 3D architecture of nephrocytes were evaluated from their reconstruction images obtained from the series of sectional FIB-SEM images (see **Fig. S4** for further details of this technique).

Sectional FIB-SEM Images of Nephrocytes in Decapods

In the species examined, nephrocytes commonly existed in the lumen of the branchial efferent vessels, which transport the oxygenated hemolymph to the pericardial sinus surrounding the heart.

The contrast-inverted FIB-SEM images achieved a quality that was comparable to conventional transmission electron microscopy images (**Fig. S5**). Like in *D. melanogaster*, nephrocytes exhibited numerous fine foot processes and slit diaphragms bridging between them in the five decapod species. Nephrocytes also possessed numerous endosome and lysosomes, which corresponded to the isolation function of toxic materials from hemolymph in nephrocytes.

3D Architecture of Nephrocytes in Decapods

The 3D architectures of nephrocytes were clearly visualized by the reconstruction images from the serial sectional FIB-SEM images. The findings were somewhat complicated since the nephrocytes exhibited different features among the examined species. We thus first overviewed their 3D architecture (**Figs. 2, 3**) and then described the detail findings (**Figs. 4–11**).

Overview

The nephrocytes were organized in each species at various levels: solitary/disjointed cells in hermit crab (like in *Drosophila* nephrocytes) (**Fig. 2e1, g1**); connected body in mitten crab (**Fig. 2f1**); epithelioid in crayfish (**Fig. 2d1**); epithelial sac with narrow lumen in lobster (**Fig. 2c1**); epithelial sac with obvious lumen in prawn (**Fig. 2b1**). The epithelial sac was quite similar to the podocyte-based coelomic sacs in invertebrate nephridial system (**Fig. 2a1**).

The foot processes were formed by different styles in nephrocytes: infolding and protrusion styles. In the infolding style, the foot processes were formed by the infolding/invagination of the basal plasma membrane, and the slit diaphragm was formed between the foot processes of the same cell as an autocellular junction (**Fig. 2e2, f2**), as found in the *Drosophila* nephrocytes (**Fig. 2g2**). In the protrusion style, the foot processes were formed by the cytoplasmic extension, and the slit diaphragm was formed between the foot processes of adjacent cells as an intercellular junction (**Fig. 2b2, c2, d2**), as found in the eucoelomate podocytes (**Fig. 2a2**).

The arrangement of foot processes was largely different between *Drosophila* and decapods. The *Drosophila* nephrocytes exhibited a washboard-like pattern, as reported previously (**Fig. 3a, d**) (Kawasaki et al., 2019); the decapod nehrocytes exhibited an interdigitating pattern. The interdigitating pattern was further divided into intercellular interdigitating (ICI) pattern (**Fig. 3b**) and autocellular interdigitating (ACI) pattern (**Fig. 3c**). The ICI pattern was found in the crayfish, lobster, and prawn, in which nephrocytes were organized into the epithelioid or epithelial sac. The foot processes were interdigitated between adjacent nephrocytes (**Fig. 3h–j**) like in podocytes (**Fig. 3g**). The ACI pattern was found in the hermit and mitten crabs, in which nephrocytes existed as solitary cells and connected body, respectively. The basal surface of 20–30 foot processes continued to form an “island”, and the foot processes were interdigitated between the adjacent islands within the same nephrocyte (**Fig. 3e, f**).

Viewing on the phylogenetic tree of decapod crustaceans, in Anomura and Brachyura (“*crab*”-called decapods), which are highly specialized groups in Decapoda, the nephrocytes were not organized into an epithelium, and the foot processes were formed by the infolding style and arranged as the ACI pattern (**Fig. 2e1–3, f1–3**). While in Dendorobrachiata, Achelata, and Astacidea (“*shrimp*”-shaped decapods), the

nephrocytes were organized into an epithelioid or epithelial sac, and the foot processes were formed by the protrusion style and arranged as the ICI pattern (**Fig. 2b1–3, c1–3, d1–3**).

The structural features peculiar to each species were described in the following sections.

Hermit crab (in comparison with D. melanogaster)

Like in *Drosophila*, nephrocytes were individually surrounded by basement membrane (**Fig. 4a, c**), and thus the nephrocytes existed as solitary cells without forming intercellular connection. The basal surface of nephrocytes was occupied by foot processes, which were formed by the infolding style and arranged as the ACI pattern (**Fig. 4d, d'**). The basal surface of 20 to 30 foot processes continued to form an island (green, blue, and yellow regions in **Fig. 4d'**). The adjacent islands were generally interdigitated by foot processes; however, the foot processes of the same island lay side by side in some regions (asterisk in **Fig. 4d'**).

In *Drosophila*, the foot processes, which were also formed by the infolding style, ran linearly and their both ends were usually anastomosed to the neighboring foot processes, resulting that the foot processes was arranged as the washboard-like pattern (**Fig. 4b**).

Mitten crab

Multiple nephrocytes formed a connected body similar to streptococcus bacteria in shape (**Fig. 5a, a', b**). The connected body was surrounded by a basement membrane *en bloc*. The adjacent nephrocytes were in close contact with each other via planar intercellular junction without intercellular space (arrowheads in **Fig. 5c**). The contacting membrane between adjacent cells was partially lost to form cytoplasmic continuity, resulting that the connected body formed a syncytium (arrows in **Fig. 5a', c, c'**).

The basal surfaces were occupied by foot processes, which were formed by the infolding style and arranged as the ACI pattern (**Fig. 5d**). The basal surface of 20 to 30 foot processes continued to form an island (red and blue regions in **Fig. 5d'**). The adjacent islands were generally interdigitated by foot processes; however, the foot processes of the same island lay side by side in some regions (asterisks in **Fig. 5d'**).

Crayfish

Multiple nephrocytes formed an epithelioid, which was like an epithelial sac without lumen (**Fig. 6a**). The epithelioid was individually surrounded by a basement membrane *en bloc*. The cell body of adjacent nephrocytes were closely apposed and connected via numerous spotty intercellular junctions (arrows in **Fig. 6b, c**) that were structurally different from the slit diaphragm between foot processes (arrowheads in **Fig. 6d**). Like in mitten crab, the contacting membrane between adjacent cell bodies was partially lost to form cytoplasmic continuity (arrows in **Fig. 6b, b'**), resulting that the epithelioid formed a syncytium.

The basic architecture was similar between crayfish nephrocytes and vertebrate podocytes. The cell body of nephrocyte projected primary processes, which typically exhibited a rounded shape (**Fig. 7b, d'**). The primary processes got under the cell body of adjacent nephrocytes, resulting that the primary processes formed their impressions on the cell body of the adjacent nephrocytes (dotted line in **Fig. 7c**).

The foot processes were formed by the protrusion style. Numerous fine foot processes were protruded from both the cell bodies and primary processes via the RLPs (yellowish-white in **Fig. 7c, d**) like in the vertebrate podocytes (**Fig. S1**). The foot processes were interdigitated between neighboring nephrocytes, resulting that the foot processes were arranged as the ICI pattern.

Lobster

Multiple nephrocytes formed an epithelial sac with a narrow lumen (**Fig. 8a, b**). The epithelial sac was in contact with the internal wall of the efferent branchial vessels (**Fig. 8b**). The contacting region to the vessel wall was altered into the flattened-shaped cells (green cells in **Fig. 8a, b**), which were similar to the parietal epithelial cells of Bowman's capsule in the vertebrate kidney

The cell body of adjacent nephrocytes were connected via numerous spotty intercellular junctions (arrows in **Fig. 8c**) that were structurally different from the slit diaphragm between foot processes (arrows in **Fig. 8d**). Unlike in crayfish, nephrocytes did not form the cytoplasmic continuity.

The cell body of nephrocyte was divided into two to four massive parts (asterisks

in **Fig. 8e**), one of which was contain a nucleus. The massive parts were interdigitated between adjacent nephrocytes. The foot processes were formed by the protrusion style. From each massive parts, numerous fine, long foot processes were protruded via the RLPs (**Figs. 8f, 8g, 9a**) and interdigitated between adjacent nephrocytes, resulting that the foot processes were arranged as the ICI pattern.

In lobster, the RLPs were partially retracted (arrowheads in **Fig. 9a**), resulting that the two foot processes on both sides of retracted RLP were closely apposed (**Fig. 9b1–3**) or connected to form an autocellular junction (**Fig. 9c1, c2**). Such contact between foot processes at their tips are not found in normal podocytes in vertebrates.

Prawn

Multiple nephrocytes formed a large epithelial sac with an obvious lumen (**Fig. 10a, b**). The epithelial sac entirely lined the internal wall of the efferent branchial vessels. Like in lobster, its contacting region to the vessel wall was formed by the flattened-shaped cells (green cells in **Fig. 10a, c, f**).

The cell body of adjacent nephrocytes were connected via spotty intercellular junctions (arrows in **Fig. 10d**) that were structurally different from the slit diaphragm between foot processes (arrowheads in **Fig. 10e**). Intercellular space between nephrocytes was widely opened, thus the nephrocytes did not form the cytoplasmic continuity.

The cell body of nephrocyte was divided into two massive parts, one of which was contain a nucleus—typically the cell body is a horseshoe magnet in shape (**Fig. 11a, b**). The massive parts were interdigitated between adjacent nephrocytes (**Fig. 11a**). The foot processes were formed by the protrusion style. From each massive parts, numerous fine, long foot processes were protruded via the RLPs (**Fig. 11e1–3**) and interdigitated between adjacent nephrocytes, resulting that the foot processes were arranged as the ICI pattern. Like in lobster, the RLPs were partially retracted (arrowheads in **Fig. 11e3**).

DISCUSSION

Decapod Nephrocytes Filled a Gap in Evolutionary Diversity of Filtration Epithelium

FIB-SEM tomography, including a reconstruction technique, clearly visualized the structural diversity of decapod nephrocytes in two aspects, tissue organization and cellular architecture. The decapod nephrocytes showed the several steps of tissue organization from the solitary cells, as found in the *Drosophila* nephrocytes, to the epithelial sac with an obvious lumen, as found in the podocyte-based coelomic sac of eucoelomate. The basic architecture of nephrocytes was highly likely to be determined by the level of tissue organization of them. In crayfish, lobster, and prawn, nephrocytes were organized into an epithelial sac and the foot processes of nephrocytes were formed by the protrusion style, like podocytes (**Fig. S6c**). In mitten and hermit crabs, nephrocytes were not organized into an epithelium and the foot processes were formed by the infolding style like in *Drosophila*; however, the foot processes were arranged as the interdigitating pattern like podocytes (**Fig. S6b**). The present findings indicated the decapod nephrocytes exhibited more highly structural similarity to podocytes than previously known in the *Drosophila* nephrocytes—they filled an enormous gap between the solitary nephrocytes in *Drosophila* and the epithelium-forming podocytes, which could be called a "*missing link*" in the evolutionary diversity of nephrocytes and podocytes.

Furthermore, due to this continuity between nephrocytes and podocytes, now it becomes necessary to clarify the definition of nephrocytes. Here we propose a definition of nephrocytes: "*Nephrocytes, a kind of highly-specialized podocyte, form the foot processes linked by slit diaphragms like podocytes, but they are not involved in the production of primary urine because of no direct connection to the modulating tubules*".

Relation among Nephrocytes, Nephridial System, and Coelom

In Arthropoda, including Crustacea, a set of the podocyte-based coelomic sac and nephridium plays a role in excretion as the nephridial system (**Fig. S1c, c'**) (Ruppert and Smith, 1988). The nephridial system in crustaceans is associated with segmental appendages, which have undergone various modifications in individual body segments, such as antennae, maxillipeds, perepods, and pleopods (Ax, 2000; Ruppert et al.,

2003). In decapod crustaceans, a pair of nephridial system, called antennal/green gland, is associated with the second antennae, and the terminal ends of them open on the exoskeleton near the base of the antennae (Longshaw and Stebbing, 2016). The gills are also derived from the segmental appendages (perepods) in decapod crustaceans, implying that the coelomic-sac primordial cells enter into the gills via their vascular system and differentiate at the various level of tissue organization within the gill.

Some crustaceans in Cephalocarida, Syncarida, Copepoda, and Isopoda possess the rudimentary coelomic sac without excretory modulating tubules, which are associated with the segmental appendages (Hessler and Elofsson, 1995; Hosfeld and Schminke, 1997; Wägele and Walter, 1990). From the conventional electron microscopy-based analyses, the rudimentary coelomic sac is considered to be formed by podocytes, which are called “segmental, extranephridial podocytes”—although, if our new definition of nephrocyte is adapted, these podocytes should be referred to nephrocytes. The epithelial sac of nephrocytes found in crayfish, lobster and prawn is highly likely to correspond to these rudimentary coelomic sac.

Nephrocyte Architecture in Other than Crustacea

Nephrocytes exist in the limited eucoelomate phyla, Arthropoda, Onycophora, and Mollusca (Crossley, 1984; Haszprunar, 1996; Seifert and Rosenberg, 1977). The two dimensional ultrastructure of nephrocytes has been reported in a variety of species belonging to these phyla (Boer and Sminia, 1976; Crossley, 1972; Goodman and Cavey, 1990; Kokkinopoulou et al., 2014)(+Refs?). In several kinds of insects, nephrocytes have been reported to possess multiple nuclei (Crossley, 1984). However, it is unclear whether such nephrocytes possess multiple nuclei per cell or if multiple nephrocytes form the connected body, epithelioid, or epithelial sac as found in decapod branchial nephrocytes.

In Mollusca, solitary nephrocytes, also referred to rhogocytes and pore cells, are disseminated broadly in mantle and muscular tissues (Haszprunar, 1996) The 3D architecture of molluscan nephrocytes has not been elucidated so far; however, it is likely to be similar to that of the *Drosophila* nephrocytes by viewing a numerous transmission electron microscopy images reported in the previous researchers (Boer

and Sminia, 1976; Kokkinopoulou et al., 2014). FIB-SEM tomography should be useful in revealing the precise 3D architecture of these nephrocytes.

Structural Diversity of Terminal Cells in Metazoan Phylogeny

Like in eucoelomates, the acoelomates and pseudocoelomates, which form no body cavity lined with mesothelium, produce the primary urine using the terminal cells of protonephridia as the filtration epithelial cells (**Fig. S1a, a'**) (Wilson and Webster, 1974). The terminal cells show ridiculous diversity in structure among taxonomic groups (Kieneke et al., 2008; Rohde, 2001). For instance, in some planarians, the terminal cell is shaped like a test tube with numerous rectangular filtration fenestrations on its cytoplasmic wall (Ishii, 1980; Nakamura et al., 2014); in puriaplus, the multiple terminal cells form an epithelial sheet with interdigitation like podocytes (Kümmel, 1964). It is difficult to evaluate the 3D ultrastructure of terminal cells by conventional electron microscopy, because the terminal cells are almost completely enwrapped by the basement membrane like nephrocytes. FIB-SEM tomography should be also useful in revealing the precise 3D architecture of terminal cells and in subsequently elucidating the spectrum of structural diversity of filtration epithelial cells including terminal cells, podocytes, and nephrocytes.

CONCLUSION

FIB-SEM tomography is a powerful tool for analyzing the 3D architecture of nephrocytes in more detail than previously possible using conventional electron microscopy. Nephrocytes in decapod crustaceans filled the enormous gap in the evolutionary diversity of podocytes and nephrocytes. We thus conclude that the nephrocyte is a part of spectrum of structural diversity in filtration epithelium

MATERIALS AND METHODS

Animals

Decapod crustaceans

Three species of marine-water decapods, prawn (*Marsupenaeus japonicus*), lobster

(*Panulirus japonicus*), and hermit crab (*Aniculus miyakei*), were collected in the Pacific coast area of Japan and were purchased from a local fish store. Two species of fresh-water decapods, crayfish (*Procambarus clarkii*) and mitten crab (*Eriocheir japonica*), were collected in the West Japan and were purchased from a local pet shop. The gills were isolated from the animals under anesthesia using a eugenol-based anesthetic agent FA100 (DS Pharma Animal Health, Osaka, Japan). The isolated gills of marine- and fresh-water decapods were fixed in 2.5% glutaraldehyde solution buffered with 0.1 M and 0.2 M phosphate buffer (PB), respectively. The fixed samples were further immersed in the same fixative solution and stored at 4°C.

Drosophila melanogaster

Drosophila melanogaster cultures and crosses were performed using standard fly food, and the flies were raised at 25°C. The adults of Canton-S strain were used to analyze the normal 3D structure of the pericardial nephrocytes. Flies were hydrophilized using 0.1% Triton X-100/0.1 M PB after anesthesia with CO_2 gas. Files were dissected to isolate heart and nephrocytes with dorsal body wall in 2.5% glutaraldehyde solution buffered with 0.1 M PB. The samples were further immersed in the same fixative solution and stored at 4°C.

Rats

The 3D ultrastructure of podocytes from adult (10-week-old, male) Wistar rats (Charles River Japan, Yokohama, Japan) was compared with that of the brachial nephrocytes. The rats were perfused (under anesthesia using pentobarbital) with physiological saline and subsequently 2.5% glutaraldehyde fixative that was buffered with 0.1 M PB. The fixed kidneys were further immersed in the same fixative and stored at 4°C These procedures were approved by the Institutional Animal Care and Use Committee of Juntendo University School of Medicine (approval no. 300226) and were carried out in accordance with the Guidelines for Animal Experimentation of Juntendo University School of Medicine.

Combinatorial Heavy Metal Staining for FIB-SEM Tomography

The fixed samples were processed using a combinatorial heavy metal staining protocol.

This protocol was designed to enhance the signal for the backscatter electron imaging of epoxy-resin-embedded mammalian tissue at low accelerating voltages. In brief, the samples were successively immersed in 1% osmium tetroxide that contained 1.5% potassium ferrocyanide in 0.1 M cacodylate buffer for 1 h on ice, 1% low molecular weight tannic acid (Electron Microscopy Sciences, Hatfield, PA) in 0.1 M cacodylate buffer for 4 h at 25°C, 2% aqueous osmium tetroxide for 30 min at 25°C, and 1% aqueous uranyl acetate overnight at 25°C. The samples were then dehydrated with a graded series of ethanol, and were embedded in epoxy resin, Oken Epok 812 (Okenshoji, Tokyo, Japan). For the detailed protocol of sample preparation, see Miyaki et al. (2020a, b).

Acquisition of Serial Block-face Images Using FIB-SEM Tomography

Serial FIB-SEM images were obtained at 30 nm increments with a backscattered electron detector at a 2.0 kV acceleration voltage using a Helios Nanolab 660 FIB-SEM (Thermo Fisher Scientific, Waltham, MA, USA). The pixel size of each FIB-SEM image was 13.5 × 17.1 × 50 nm/pixel (width × height × depth). The pixel dimensions for a recorded image was 3072 × 2048 pixels. Thus, the dimension of serial imaging by FIB-SEM was 41.5 × 35.0 × 20.0–35.0 μm (width × height × depth). The new surface for serial FIB-SEM imaging was generated by FIB-milling using a 0.77 nA beam current, where gallium ions were accelerated with a voltage of 30 kV.

Data Processing for 3D Reconstruction

The 3D reconstruction of nephrocytes was performed using AMIRA 6.1 Software (Thermo Fisher Scientific) on a MousePro-W994DQP5X professional workstation (Mouse Computer Co. Ltd., Tokyo, Japan). We used a Cintiq 27QHD interactive pen display for the segmentation procedure (Wacom, Tokyo, Japan).

ACKNOWLEDGMENTS

The authors thank Mr. Takanobu Ishimura (Maxnet Co., Ltd., Tokyo, Japan) for the technical lecture on Amira software.

AUTHOR CONTRIBUTIONS

K.I. designed the experiments. K.I. and S.K. obtained the serial FIB-SEM images. A.M. performed fly bleeding. T.M., Y.K., and K.I. performed 3D reconstruction. T.M., T.S., and K.I. analyzed the experimental data. T.M. and K.I. prepared the figures and wrote the main manuscript text. All authors reviewed the manuscript.

COMPETING INTERESTS

The authors declare there are no competing financial interests.

FUNDING

This work was supported in part by the Japan Society for the Promotion of Science (JSPS) KAKENHI (grant nos. JP15K18960, JP17K08521 to KI).

FIGURE REGENDS

Figure 1. Large structural distinction between eucoelomate epithelium-forming podocytes and *Drosophila* solitary nephrocyte.

(**a1–a3**) Podocytes in eucoelomates. Podocytes (**P**) form a filtration epithelium, through which the primary urine is produced (**a1**). The primary urine is excluded via a nephridium. Unlike in the *Drosophila* nephrocytes, the foot processes are formed by the cytoplasmic protrusion from the cell periphery (protrusion style) and are interdigitated each other between the adjacent podocytes (**a2**). The podocyte slit diaphragms between the foot processes thus are regarded as an intercellular junction (**a3**). Individual nephrocytes and podocytes are shown by different colors (purple and green). (**b1–b3**) Nephrocytes in fruit fly (*Drosophila melanogaster*). Individual nephrocytes (**N**) are completely enwrapped by basement membrane (yellow line) (**b1**). The foot processes are formed by the infolding of basal plasma membrane (infolding style) (**b2**). The slit diaphragms are bridged between the foot processes from the same nephrocyte, thus they are regarded as an autocellular junction (**b3**). **BM**, basement

membrane; **FP**, foot process; **SD**, slit diaphragm.

Figure 2. Architecture of decapod nephrocytes in relation to phylogeny.

Decapod branchial nephrocytes exhibit more highly similarity to the eucoelomate epithelium-forming podocytes (**a1–3**) in comparison with the *Drosophila* solitary nephrocytes (**g1–3**). These similarities are found in the aspects of tissue organization (**a1–g1**), styles of foot process formation (**a2–g2**), and pattern of foot process arrangement (**a3–g3**). (**b1–3, c1–3, d1–3**) In prawn, lobster, and crayfish, the nephrocytes are organized into a closed epithelial sac or an epithelioid. The foot processes are formed by the protrusion style and are arranged as the intercellular interdigitation (ICI) pattern like in podocytes (**a2, a3**). (**e1–3, f1–3**) In hermit and mitten crabs, the nephrocytes are not organized into an epithelium. The foot processes are formed by the infolding style like in *Drosophila* nephrocytes (**g2**); however they are arranged as the autocellular interdigitation (ACI) pattern like in podocytes (**a3**).

Figure 3. Patterns of foot process arrangement in nephrocytes.

(**a–c**) Three patterns of foot process arrangement are recognized in nephrocytes. The washboard-like (WB) pattern is found in Fruit fly (*Drosophila melanogaster*), as reported previously (Kawasaki et al., 2019) (**a**). In decapods, the foot processes are arranged as the interdigitation pattern (**b, c**). In the hermit and mitten crabs, the foot processes from the same cell are interdigitated each other (autocellular interdigitation (ACI) pattern) (**b**); in crayfish, lobster, and prawn, the foot processes are interdigitated between the adjacent cells (intercellular interdigitation (ICI) pattern) (**c**). (**d–f, h–j**) The basal surface of 3D reconstructed nephrocytes in decapods. Individual nephrocytes are painted in different colors (purple and green). The arrangement of foot processes is clearly visible on the basal surface of 3D reconstructed nephrocytes. (**g**) The basal surface of 3D reconstructed podocyes in rat. The foot processes are arranged as the ICI pattern. Scale bars: 500 nm.

Figure 4. Nephrocytes in fruit fly and hermit crab.

(**a, b**) Fruit fly (*Drosophila melanogaster*). (**c, d, d'**) Hermit crab. (**a, c**) FIB-SEM sectional images. Individual nephrocytes of both species are entirely surrounded by

basement membrane (yellow lines), and thus the nephrocytes exist as solitary cells without forming intercellular connection each other. (**b, d**) The basal surface of reconstructed nephrocytes. The basal surface of foot processes, which adhere to the basement membrane, is painted by whitish-purple. The foot processes are formed by the infolding style in both species; however, the pattern of their arrangement are different between them. (**b**) In fruit fly, the foot processes run linearly and their both ends are usually anastomosed to the neighboring foot processes—the foot processes are arranged as the washboard-like pattern. (**d**) In hermit crab, the foot processes of the same nephrocyte are interdigitated, but not between the adjacent cells—they are arranged as the autocellular interdigitation (ACI) pattern. (**d'**) The basal surface of 20 to 30 foot processes continued to form an island (green, blue, and yellow regions) in hermit crab. The adjacent islands were generally interdigitated by foot processes. In some regions, the foot processes of the same island lay side by side (asterisk in **d'**). Scale bars: 500 nm in **a, c**; 1 μm in **b, d**. The reconstructed nephrocytes (**b** and **d**) are also shown in **Movies S2** and **S3**.

Figure 5. Nephrocytes in mitten crab.

(**a, a'**) Schematic drawings. (**a**) Multiple nephrocytes (**N**) form a connected body similar to streptococcus bacteria in shape. (**a'**) The connected body is surrounded by a basement membrane *en bloc* (yellow line). The contacting membrane of adjacent nephrocytes is partially lost to form a cytoplasmic continuity, resulting that the connected body of nephrocytes form a syncytium (arrows). (**b, c, c'**) FIB-SEM sectional images. (**b**) The four nephrocytes (**N1–N4**) form a connected body. (**c**) The adjacent nephrocytes (**N1, N2**) are in close contact with each other via planar intercellular junction without intercellular space (arrowheads). The contacting membrane between adjacent cells is partially lost to form a cytoplasmic continuity (arrows). (**c'**) Magnification of the cytoplasmic continuity shown in **c**. (**d**) The basal surface of a reconstructed connected body. Two adjacent nephrocytes (purple and green) are shown. The foot processes from the same cell are interdigitated each other, but not between the adjacent cells—they are arranged as the autocellular interdigitation (ACI) pattern. (**d'**) The basal surface of 20 to 30 foot processes continued to form an island (yellow, red, and blue regions). The adjacent islands were generally interdigitated by

foot processes. In some regions, the foot processes of the same island lay side by side (asterisks). Scale bars: 5 μm in **b**; 1 μm in **c**; 500 nm in **c', d**. The reconstructed nephrocyte (**d**) is also shown in **Movie S4**.

Figure 6. Nephrocytes in crayfish.

(**a**) Schematic drawings. Multiple nephrocytes form an epithelioid, which is like an epithelial sac without lumen. The epithelioid is surrounded by a basement membrane *en bloc* (yellow line). (**b–d, b'**) FIB-SEM sectional images. (**b**) The border of adjacent nephrocyte cell bodies (**N1, N2**) is indicated by arrowheads. Like in mitten crab, the contacting membrane between adjacent cell bodies is partially lost to form a cytoplasmic continuity (arrows), resulting that the epithelioid of nephrocytes form a syncytium. (**b'**) Magnification of the cytoplasmic continuity shown in **b**. (**c, d**) The cell body of adjacent nephrocytes are closely apposed and connected via numerous spotty intercellular junctions (arrows in **c**), which are structurally different from the slit diaphragm between foot processes (arrowheads in **d**). Scale bars: 1 μm in **b**; 100 nm in **b', c, d**.

Figure 7. Nephrocytes in crayfish.

(**a, a'**) Reconstruction images of two adjacent nephrocytes that are painted in green and purple. The adjacent nephrocytes are interdigitated each other. There is no obvious intercellular space between them. (**b**) Apical view of a single reconstructed nephrocyte. This cell is contained by the epithelioid shown in **a, a'**. Three primary processes (**PP1–PP3**), which typically exhibit a rounded shape, are projected from the periphery of the cell body (**CB**). (**c, d**) Basal view of reconstructed nephrocytes. Two adjacent reconstructed nephrocytes are separated. The purple cell shows the basal surface of primary processes (**d**). The green cell shows the basal surface of cell body, on which the primary processes of the adjacent purple cell makes their impressions (dotted line in **c**). From the cell body and primary processes, numerous foot processes (whitish-green in **c**, whitish-purple in **d**) are protruded via ridge-like prominences (**RLP**) (yellowish-green in **c**, yellowish-purple in **d**). (**d'**) The apical view of the purple

nephrocyte shown in **d**. Scale bars: 2 μm in **a, a'**; 500 nm in **b–d**. The reconstructed nephrocytes (**b–d**) are also shown in **Movies S5** and **S6**.

Figure 8. Nephrocytes in lobster.

(**a**) Schematic drawing. Multiple nephrocytes (**N**) form an epithelial sac with a quite narrow lumen (**L**). The sac is partially altered into the flattened-shaped cells (**F**, green cells). The cytoplasmic continuity is not formed between nephrocytes. (**b–d**) FIB-SEM sectional images. (**b**) The connecting part of the nephrocytes (purple) and flattened-shaped cells (green), which are contact with the internal wall of efferent branchial vessel (**EBV**). (**c, d**) The cell bodies and primary processes of adjacent nephrocytes are closely apposed and connected via spotty intercellular junctions (arrows in **c**), which are structurally different from the slit diaphragm between foot processes (arrowheads in **d**). (**e–g, e'**) Reconstruction images of two adjacent nephrocytes that are painted in green and purple. (**e**) The luminal view of the green nephrocyte shows the cell body of nephrocyte is divided into two to four massive parts (asterisks). (**e'**) The green and purple cells are interdigitated each other by their massive parts. (**f, g**) The basal view of purple and green nephrocytes. From each massive parts, numerous fine, long foot processes (whitish-purple in **f**, whitish-green in **g**) are protruded from each massive parts. Scale bars: 2 μm in **a**; 100 nm in **c–g**. The reconstructed nephrocytes (**e–g**) are also shown in **Movie S7**.

Figure 9. Nephrocytes in lobster.

(**a–f**) Reconstruction images of two adjacent nephrocytes that are painted in green and purple. All images show the basal surface of the cells. (**a**) Numerous fine, long foot processes (whitish-purple) are protruded from a massive parts via the ridge-like prominence (yellowish-purple). (**b1–3, c1, c2**) The ridge-like prominence (RLP) is partially retracted (arrowheads in **a, b3**). Due to the retraction of RLP, the two foot processes on both sides of retracted RLP are closely apposed (arrows in **b1, b2**) or connected to form an autocellular junction (arrowheads in **c1, c2**). Scale bars: 100 nm. The reconstructed nephrocyte (**a**) is also shown in **Movie S8**.

Figure 10. Nephrocytes in prawn.

(**a**) Schematic drawing. Multiple nephrocytes (**N**) form a large epithelial sac with an obvious lumen (**L**). The sac is partially altered into the flattened-shaped cells (**F**, green cells). The cytoplasmic continuity is not formed between nephrocytes. (**b**) Semi-thin resin-section. Lumen of the epithelial sac is clearly visible in the level of light microscopy. (**c–f**) FIB-SEM sectional images. (**c, f**) The connecting part (arrows) of the nephrocytes (purple) and flattened-shaped cells (green). The flattened-shaped cells are in contact with the internal wall of efferent branchial vessel (**EBV**). (**d**) Nephrocytes contain huge lysosomes (**Ly**) (**b**). The cell body of adjacent nephrocytes are connected via spotty intercellular junctions (arrows in **d**) that are structurally different from the slit diaphragm between foot processes (arrowheads in **e**). Intercellular space (asterisks in **d, f**) is widely opened between nephrocytes. The cytoplasmic continuity is not formed between nephrocytes. **BM**, basement membrane. Scale bars: 5 μm in **b**; 1 μm in **c, d, f**; 100 nm in **e**.

Figure 11. Nephrocytes in prawn.

(**a–d**) Reconstruction images of two adjacent nephrocytes that are painted in green and purple. (**a, b**) The cell body of nephrocyte is divided into two massive parts (asterisks)—typically the cell body is a horseshoe magnet in shape (**b**). The massive parts are interdigitated between adjacent purple and green nephrocytes (**a**). (**c**) The luminal view of a massive part of purple nephrocytes. Numerous fine, long foot processes are protruded from the massive part, some of which are protruded via short, thick primary processes (**PP**). (**d**) The basal view of the green nephrocyte, numerous fine, long foot processes (whitish-green) are protruded from each massive part. (**e1–e3**) Magnification of the basal surface. The foot processes are protruded via the ridge-like prominences (RLP) (yellowish-green). The RLP is partially retracted (arrowheads in **e3**). Due to the retraction of RLP, the two foot processes on both sides of retracted RLP are closely apposed (arrows in **e1**). Scale bars: 1 μm in **a, b**; 500 nm in **c, d;** 100 nm in **e1–e3**. The reconstructed nephrocytes (**a–d**) are also shown in **Movies S9–S11**.

REFERENCES

Andrikou, C., Thiel, D., Ruiz-Santiesteban, J.A., Hejnol, A., 2019. Active mode of excretion across digestive tissues predates the origin of excretory organs. PLoS Biol 17, e3000408.

Assady, S., Wanner, N., Skorecki, K.L., Huber, T.B., 2017. New Insights into Podocyte Biology in Glomerular Health and Disease. J Am Soc Nephrol 28, 1707-1715.

Ax, P., 2000. Multicellular animals: the phylogenetic system of the metazoa Springer-Verlag, Berlin.

Boer, H.H., Sminia, T., 1976. Sieve structure of slit diaphragms of podocytes and pore cells of gastropod molluscs. Cell Tissue Res 170, 221-229.

Crossley, A.C., 1972. The ultrastructure and function of pericardial cells and other nephrocytes in an insect: *Calliphora erythrocephala*. Tissue Cell 4, 529-560.

Crossley, A.C., 1984. Nephrocytes and pericardial cells., in: Kerkut, G.A., Gilber, L.I. (Eds.), Integument, respiration and circulation., 1st ed. Pergamon Press, pp. 487-515.

Evans, D.H., 2008. Osmotic and ionic regulation: cells and animals. CRC press, London.

Fu, Y., Zhu, J.Y., Richman, A., Zhang, Y., Xie, X., Das, J.R., Li, J., Ray, P.E., Han, Z., 2017. APOL1-G1 in nephrocytes induces hypertrophy and accelerates cell death. J Am Soc Nephrol 28, 1106-1116.

Goodman, S.H., Cavey, M.J., 1990. Organization of a phyllobranchiate gill from the green shore crab *Carcinus maenas* (Crustacea, Decapoda). Cell Tissue Res 260, 495-505.

Haszprunar, G., 1996. The molluscan rhogocyte (pore-cell, Blasenzelle, cellule nucale), and its significance for ideas on nephridial evolution. J Moll Stu 62, 185-211.

Helmstädter, M., Simons, M., 2017. Using *Drosophila* nephrocytes in genetic kidney disease. Cell Tissue Res 369, 119-126.

Hessler, R.R., Elofsson, R., 1995. Segmental podocytic excretory glands in the thorax of *Hutchinsoniella macracantha* (Cephalocarida). Journal of Crustacean Biology 15, 61-69.

Heymann, J.A., Hayles, M., Gestmann, I., Giannuzzi, L.A., Lich, B., Subramaniam, S., 2006. Site-specific 3D imaging of cells and tissues with a dual beam microscope. J Struct Biol 155, 63-73.

Hosfeld, B., Schminke, H.K., 1997. Discovery of segmental extranephridial podocytes in Harpacticoida (Copepoda) and Bathynellacea (Syncarida). Journal of Crustacean Biology 17, 13-20.

Ichimura, K., Fukuyo, Y., Nakamura, T., Powell, R., Sakai, T., Janknecht, R., Obara, T., 2013. Developmental localization of nephrin in zebrafish and medaka pronephric glomerulus. J Histochem Cytochem 61, 313-324.

Ichimura, K., Fukuyo, Y., Nakamura, T., Powell, R., Sakai, T., Obara, T., 2012. Structural disorganization of pronephric glomerulus in zebrafish *mpp5a/nagie oko* mutant. Dev Dyn 241, 1922-1932.

Ichimura, K., Kakuta, S., Kawasaki, Y., Miyaki, T., Nonami, T., Miyazaki, N., Nakao, T., Enomoto, S., Arai, S., Koike, M., Murata, K., Sakai, T., 2017. Morphological process of podocyte development revealed by block-face scanning electron microscopy. J Cell Sci 130, 132-142.

Ichimura, K., Kurihara, H., Sakai, T., 2007. Actin filament organization of foot processes in vertebrate glomerular podocytes. Cell Tissue Res 329, 541-557.

Ichimura, K., Miyaki, T., Kawasaki, Y., Kinoshita, M., Kakuta, S., Sakai, T., 2019. Morphological processes of foot process effacement in puromycin aminonucleoside nephrosis revealed by FIB/SEM tomography. J Am Soc Nephrol.

Ichimura, K., Miyazaki, N., Sadayama, S., Murata, K., Koike, M., Nakamura, K., Ohta, K., Sakai, T., 2015. Three-dimensional architecture of podocytes revealed by block-face scanning electron microscopy. Sci Rep 5, 8993.

Ichimura, K., Sakai, T., 2017. Evolutionary morphology of podocytes and primary urine-producing apparatus. Anat Sci Int 92, 161-172.

Ichimura, K., Sakai, T., 2018. Acquisition and evolution of the renal glomerulus in vertebrates. Juntendo Med J 64, 37-45.

Ishii, S., 1980. The ultrastructure of the protonephridial flame cell of the freshwater planarian *Bdellocephala brunnea*. Cell Tissue Res 206, 441-449.

Kümmel, G., 1964. Die Feinstruktur der Terminalzellen (Cyrtocyten) an den Protonephridien der Priapuliden. 62:468–484. Z Zellforsch 62, 468–484.

Kawasaki, Y., Matsumoto, A., Miyaki, T., Kinoshita, M., Kakuta, S., Sakai, T., Ichimura, K., 2019. Three-dimensional architecture of pericardial nephrocytes in Drosophila melanogaster revealed by FIB/SEM tomography. Cell Tissue Res 378, 289-300.

Kieneke, A., Ahlrichs, W.H., Arbizu, P.M., Bartolomaeus, T., 2008. Ultrastructure of protonephridia in *Xenotrichula carolinensis syltensis* and *Chaetonotus maximus* (Gastrotricha : Chaetonotida): comparative evaluation of the gastrotrich excretory organs. Zoomorphology 127, 1-20.

Kokkinopoulou, M., Guler, M.A., Lieb, B., Barbeck, M., Ghanaati, S., Markl, J., 2014. 3D-ultrastructure, functions and stress responses of gastropod (*Biomphalaria glabrata*) rhogocytes. PLoS One 9, e101078.

Kriz, W., Kaissling, B., 2007. Structural organization of the mammalian kidney, in: Alpern, R.J., Hebert, S.C. (Eds.), Seldin and Giebisch's the kidney: physiology and pathophysiology, 4th ed. Academic Press, pp. 479-563.

Kubota, Y., 2015. New developments in electron microscopy for serial image acquisition of neuronal profiles. Microscopy (Oxf) 64, 27-36.

Longshaw, M., Stebbing, P., 2016. Biology and ecology of crayfish. CRC Press, London.

Miyaki, T., Kawasaki, Y., Hosoyamada, Y., Amari, T., Kinoshita, M., Matsuda, H., Kakuta, S., Sakai, T., Ichimura, K., 2020a. Three-dimensional imaging of podocyte

ultrastructure using FE-SEM and FIB-SEM tomography. Cell Tissue Res (in press).

Miyaki, T., Kawasaki, Y., Hosoyamada, Y., Amari, T., Kinoshita, M., Matsuda, H., Kakuta, S., Sakai, T., Ichimura, K., 2020b. Volume scanning electron microscopy for 3D imaging of biological ultrastructure. Juntendo Med J (in press).

Na, J., Sweetwyne, M.T., Park, A.S., Susztak, K., Cagan, R.L., 2015. Diet-induced podocyte dysfunction in *Drosophila* and mammals. Cell Rep 12, 636-647.

Nakamura, T., Takagi, S., Matsumoto, M., Tashiro, F., Sakai, T., Ichimura, K., 2014. Expression of nephrin homologue in the freshwater planarian, *Dugesia japonica*. Acta Histochem Cytochem 47, 303-310.

Ohno, N., Katoh, M., Saitoh, Y., Saitoh, S., Ohno, S., 2015. Three-dimensional volume imaging with electron microscopy toward connectome. Microscopy (Oxf) 64, 17-26.

Ohta, K., Sadayama, S., Togo, A., Higashi, R., Tanoue, R., Nakamura, K., 2012. Beam deceleration for block-face scanning electron microscopy of embedded biological tissue. Micron 43, 612-620.

Pavenstadt, H., Kriz, W., Kretzler, M., 2003. Cell biology of the glomerular podocyte. Physiol Rev 83, 253-307.

Rohde, K., 2001. Protonephridia as phylogenetic characters, in: Littlewood, D.T.J., Bray, R.A. (Eds.), Interrelationships of the platyhelminthes. Taylor and Francis, London, pp. 203-216.

Ruppert, E., Fox, R., Barnes, R., 2003. Invertebrate zoology: a functional evolutionary approach, 7th ed. Thomson Learning, Belmont.

Ruppert, E., Smith, P., 1988. The functional organization of filtration nephridia. Biol Rev 63, 231-258.

Ruppert, E.E., 1994. Evolutionary origin of the vertebrate nephron. Amer Zool 34, 542-553.

Seifert, G., Rosenberg, J., 1977. Die Ultrastruktur der Nephrozyten von *Peripatoides*

leuckarti (Saenger 1869) (Onychophora, Peripatopsidae). Zoomorphologie 86, 169-181.

Titze, B., Genoud, C., 2016. Volume scanning electron microscopy for imaging biological ultrastructure. Biol Cell 108, 307-323.

Tsang, L.M., Ma, K.Y., Ahyong, S.T., Chan, T.Y., Chu, K.H., 2008. Phylogeny of Decapoda using two nuclear protein-coding genes: Origin and evolution of the Reptantia. Molecular Phylogenetics and Evolution 48, 359-368.

Tutor, A.S., Prieto-Sanchez, S., Ruiz-Gomez, M., 2014. Src64B phosphorylates Dumbfounded and regulates slit diaphragm dynamics: *Drosophila* as a model to study nephropathies. Development 141, 367-376.

Wägele, J.W., Walter, U., 1990. Discovery of Extranephridial Podocytes in Isopods. Journal of Crustacean Biology 10, 400-405.

Weavers, H., Prieto-Sanchez, S., Grawe, F., Garcia-Lopez, A., Artero, R., Wilsch-Brauninger, M., Ruiz-Gomez, M., Skaer, H., Denholm, B., 2009. The insect nephrocyte is a podocyte-like cell with a filtration slit diaphragm. Nature 457, 322-326.

Weide, T., Vollenbroker, B., Schulze, U., Djuric, I., Edeling, M., Bonse, J., Hochapfel, F., Panichkina, O., Wennmann, D.O., George, B., Kim, S., Daniel, C., Seggewiss, J., Amann, K., Kriz, W., Krahn, M.P., Pavenstadt, H., 2017. Pals1 haploinsufficiency results in proteinuria and cyst formation. J Am Soc Nephrol 28, 2093-2107.

Wilson, R.A., Webster, L.A., 1974. Protonephridia. Biol Rev Camb Philos Soc 49, 127-160.

Zhuang, S., Shao, H., Guo, F., Trimble, R., Pearce, E., Abmayr, S.M., 2009. Sns and Kirre, the *Drosophila* orthologs of Nephrin and Neph1, direct adhesion, fusion and formation of a slit diaphragm-like structure in insect nephrocytes. Development 136, 2335-2344.

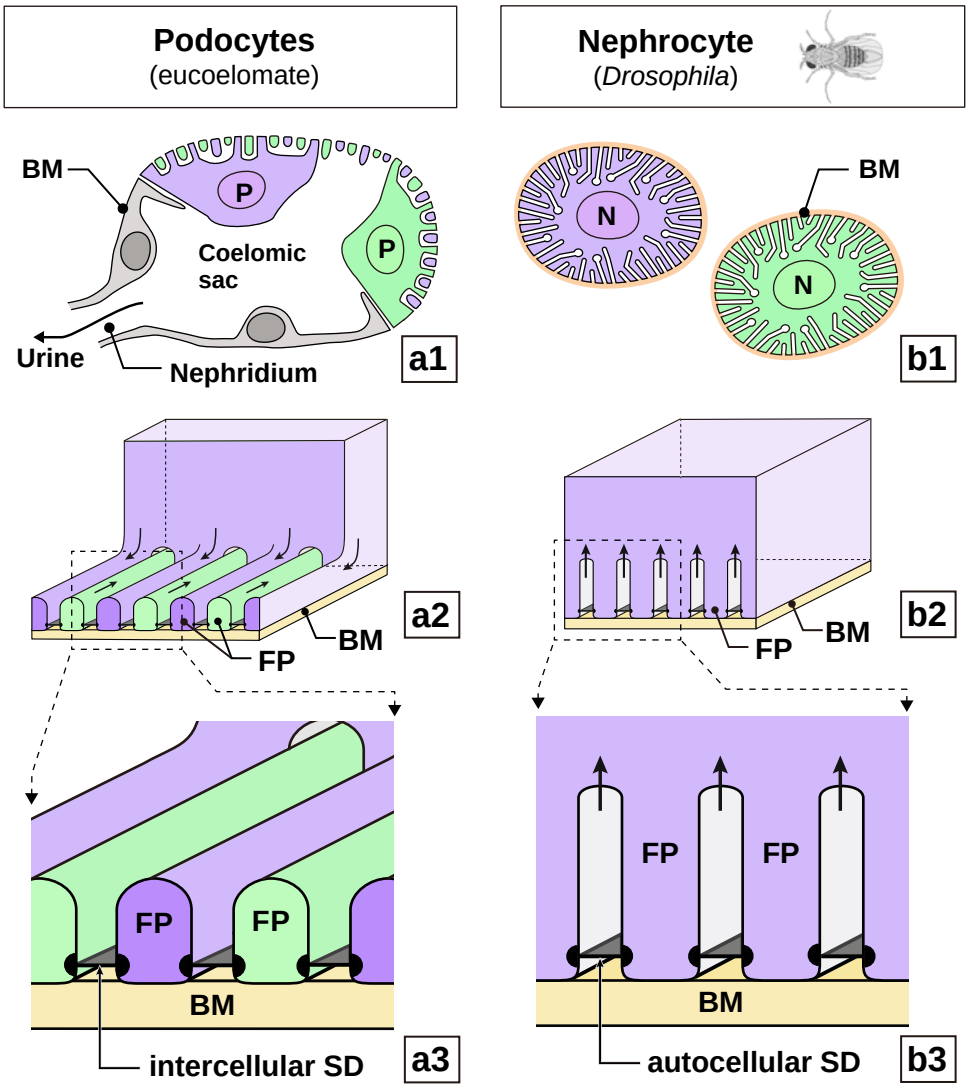

Figure 1
Miyaki et al.

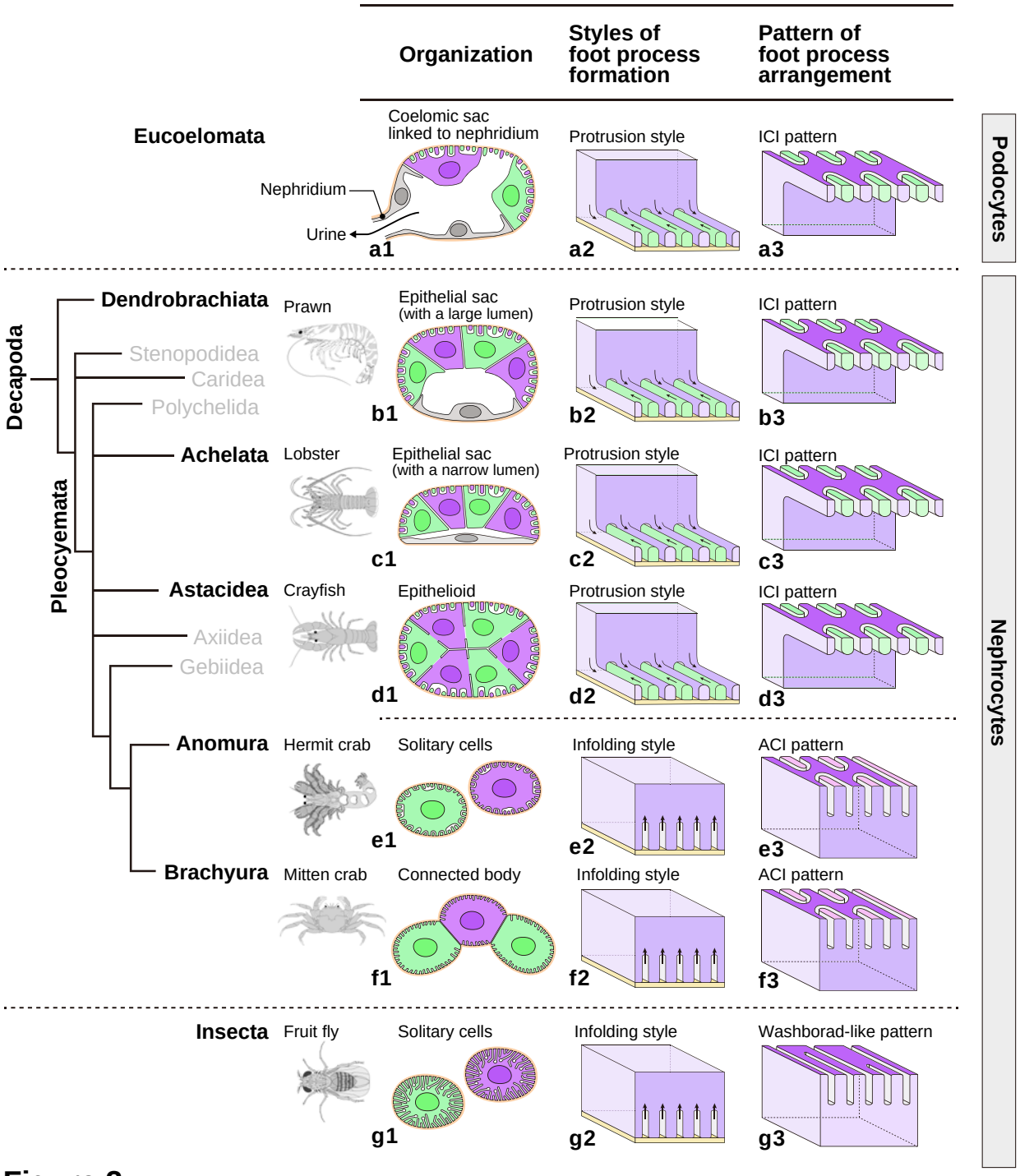

Figure 2
Miyaki et al.

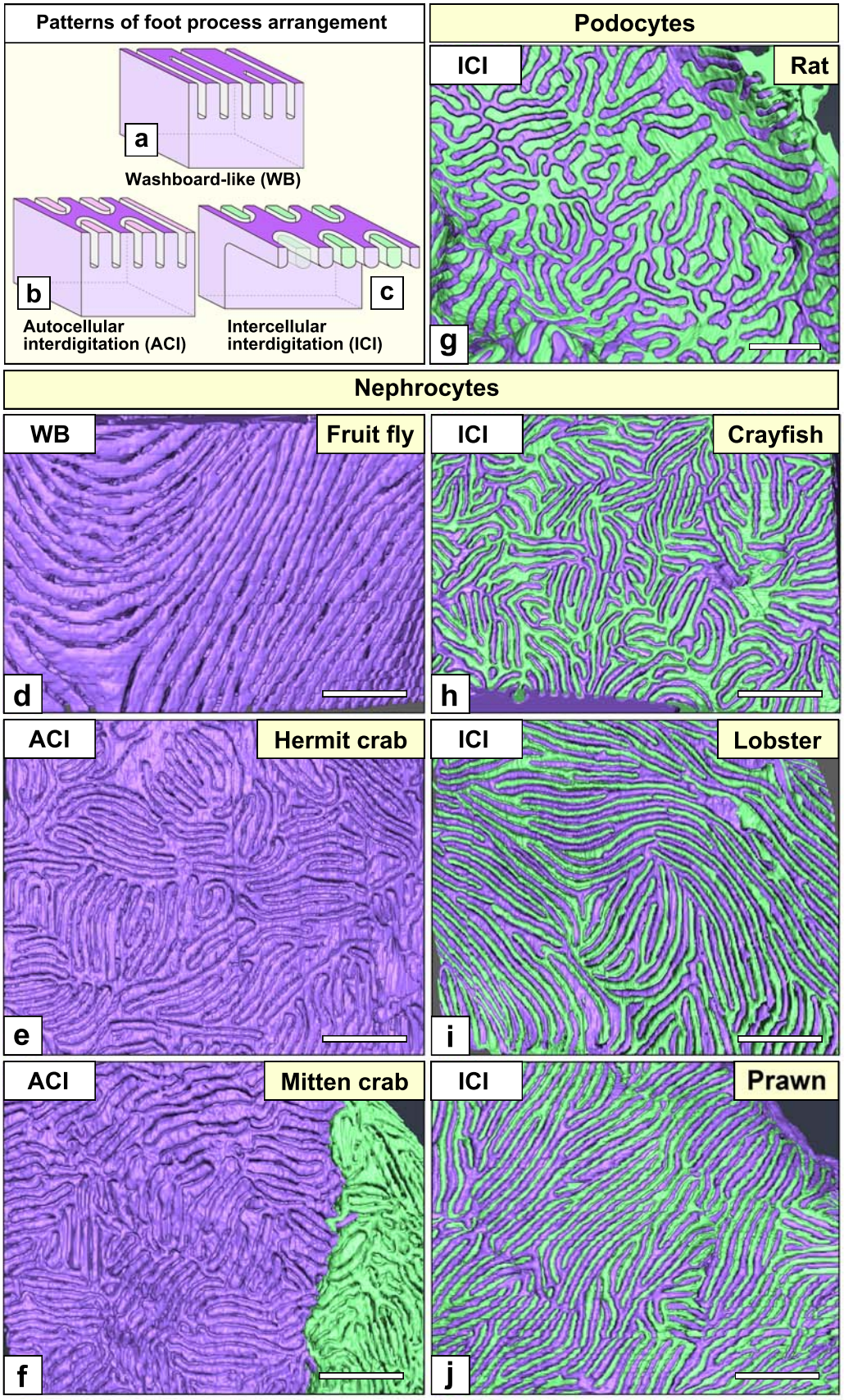

Figure 3
Miyaki et al.

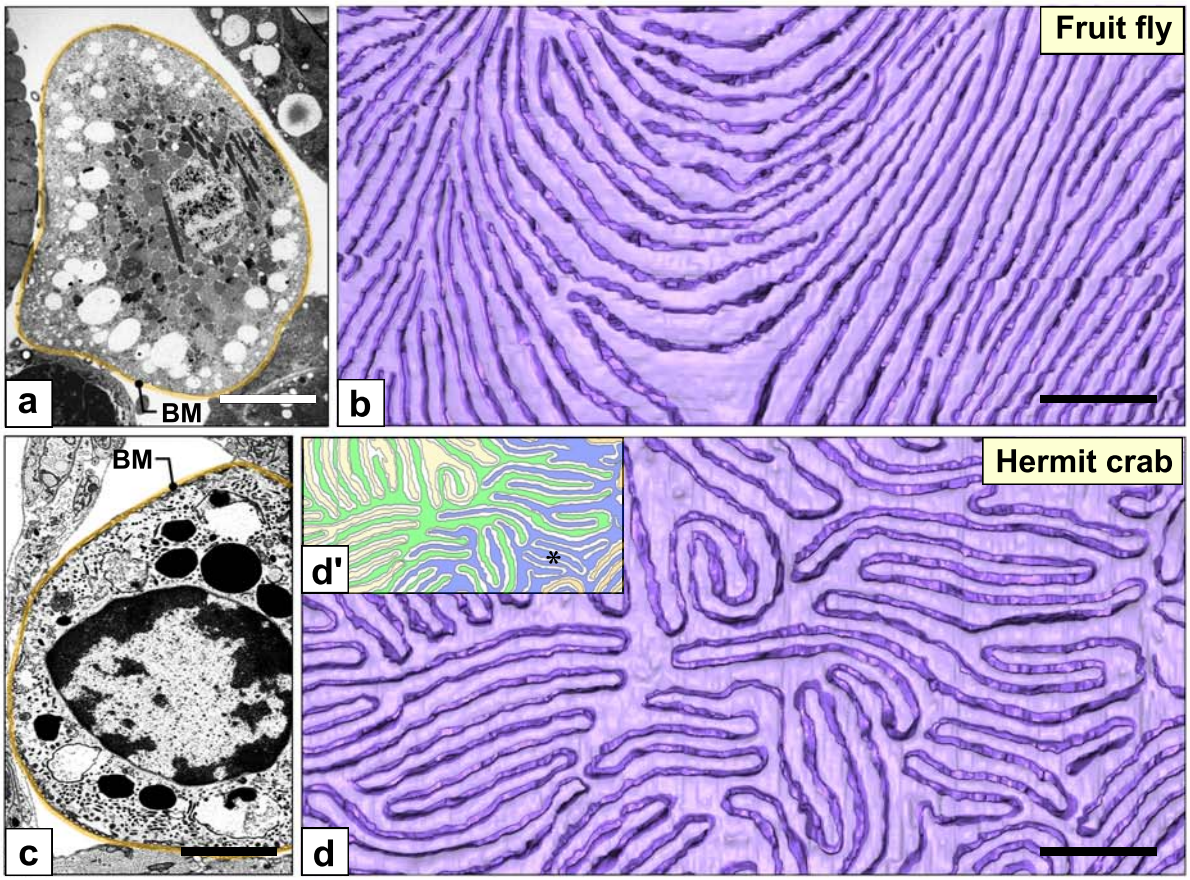

Figure 4
Miyaki et al.

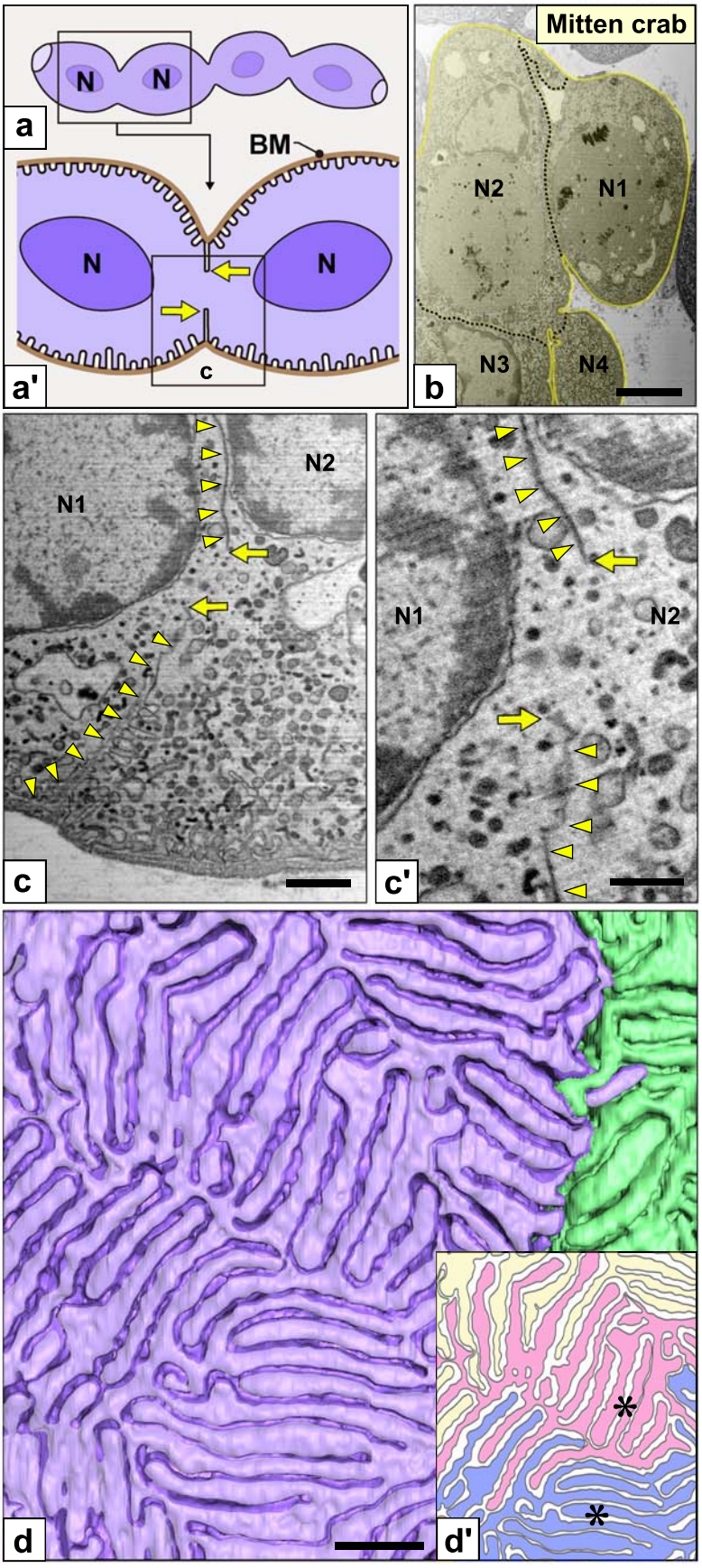

Figure 5
Miyaki et al.

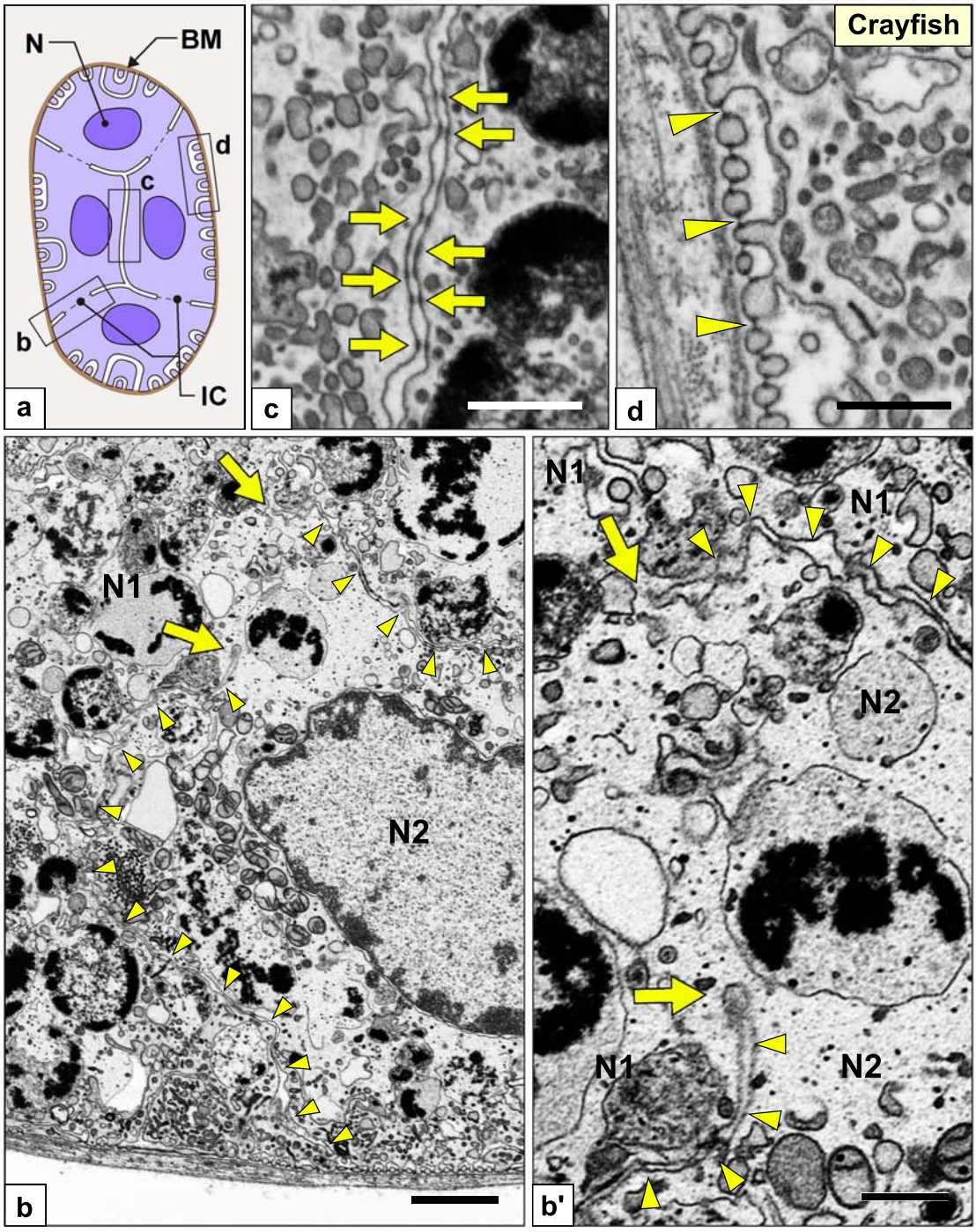

Figure 6
Miyaki et al.

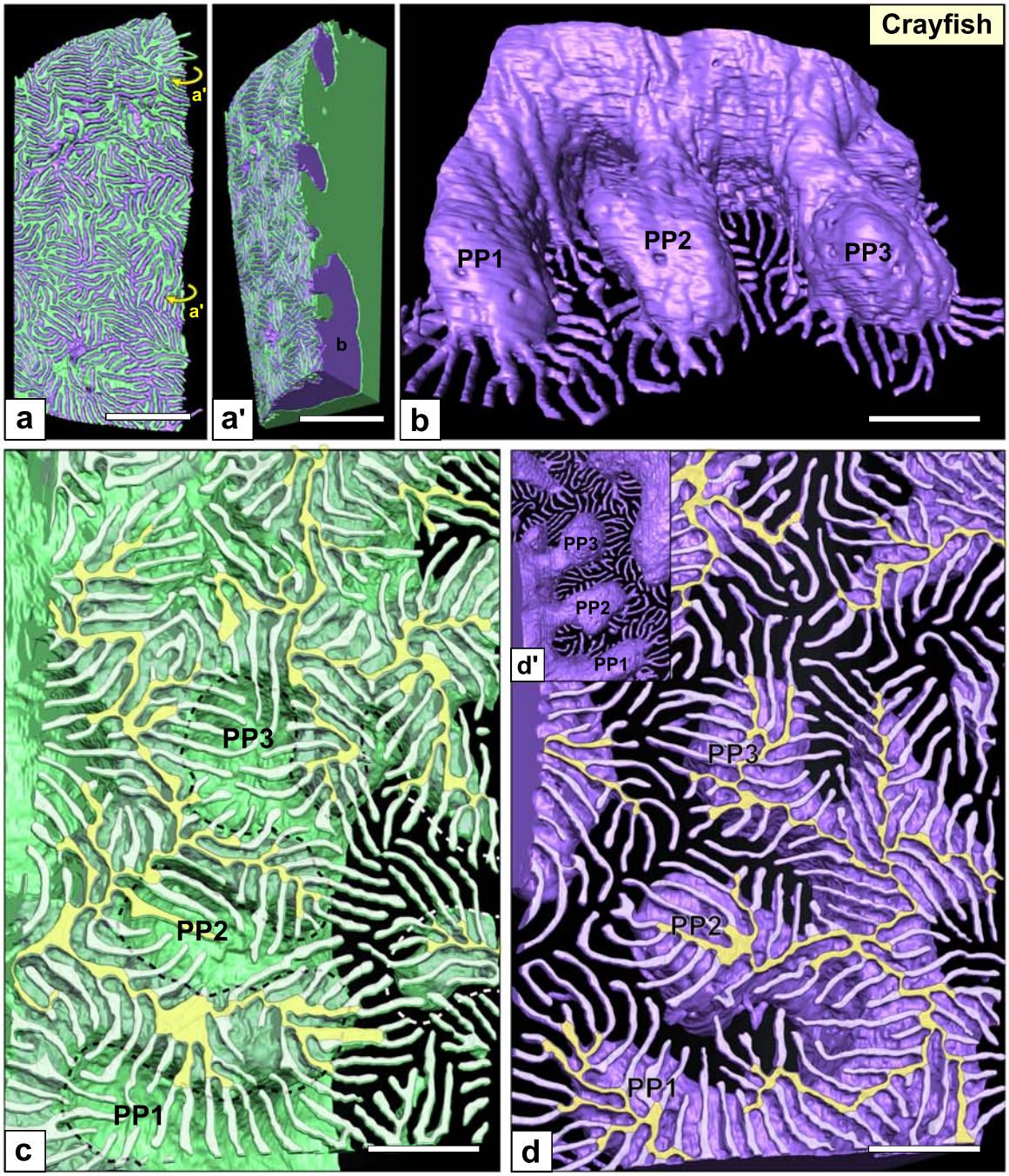

Figure 7
Miyaki et al.

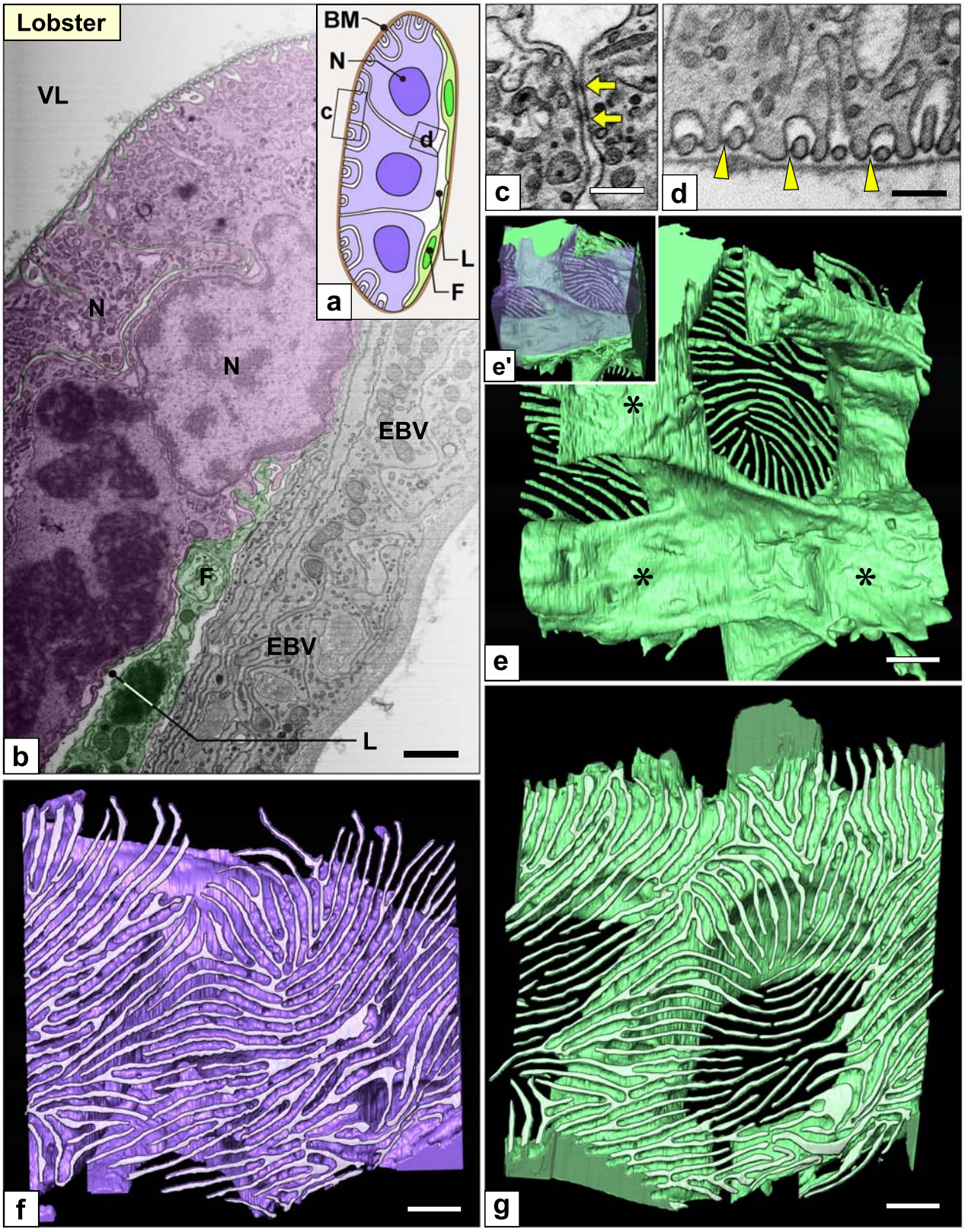

Figure 8
Miyaki et al.

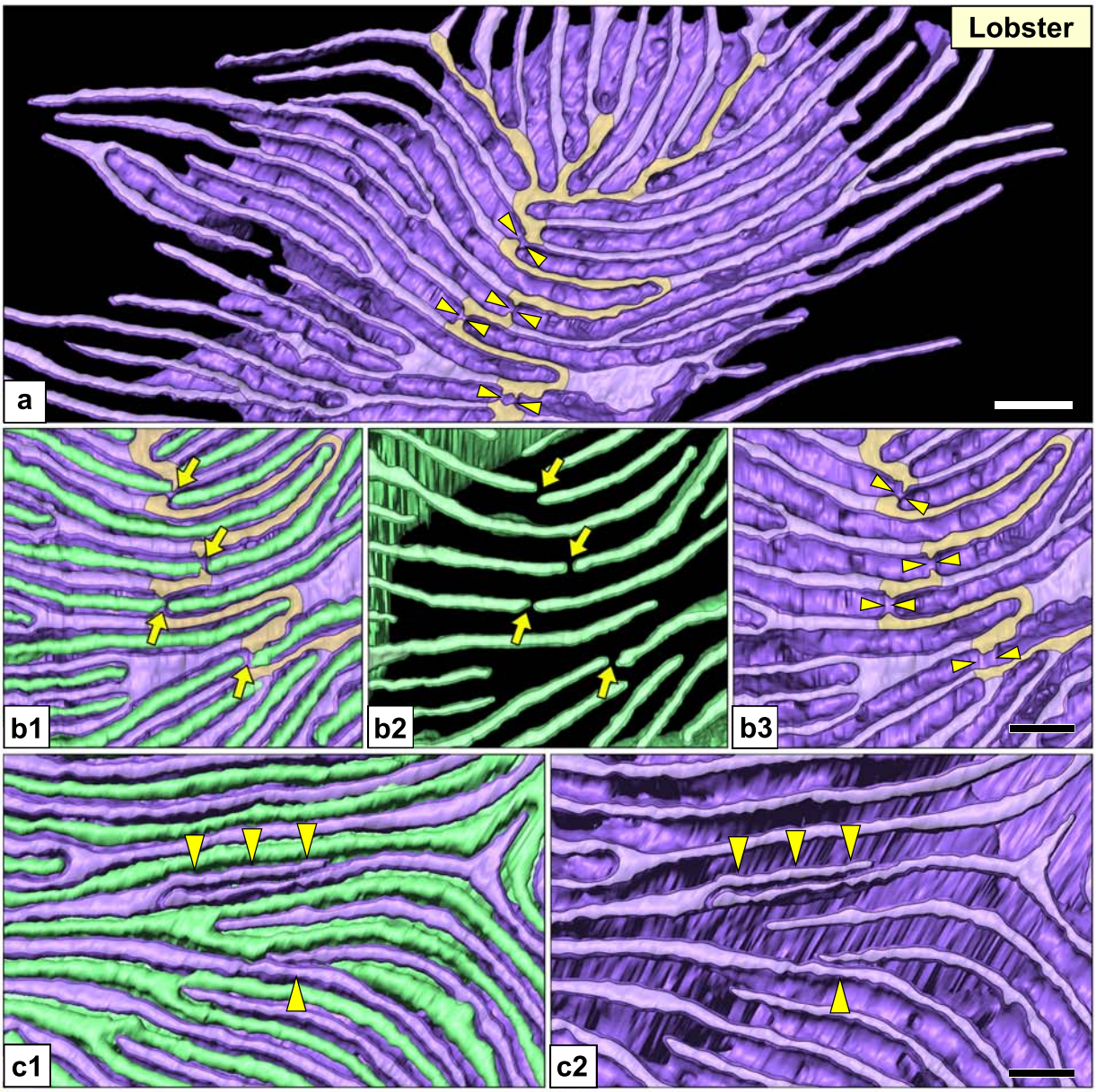

Figure 9
Miyaki et al.

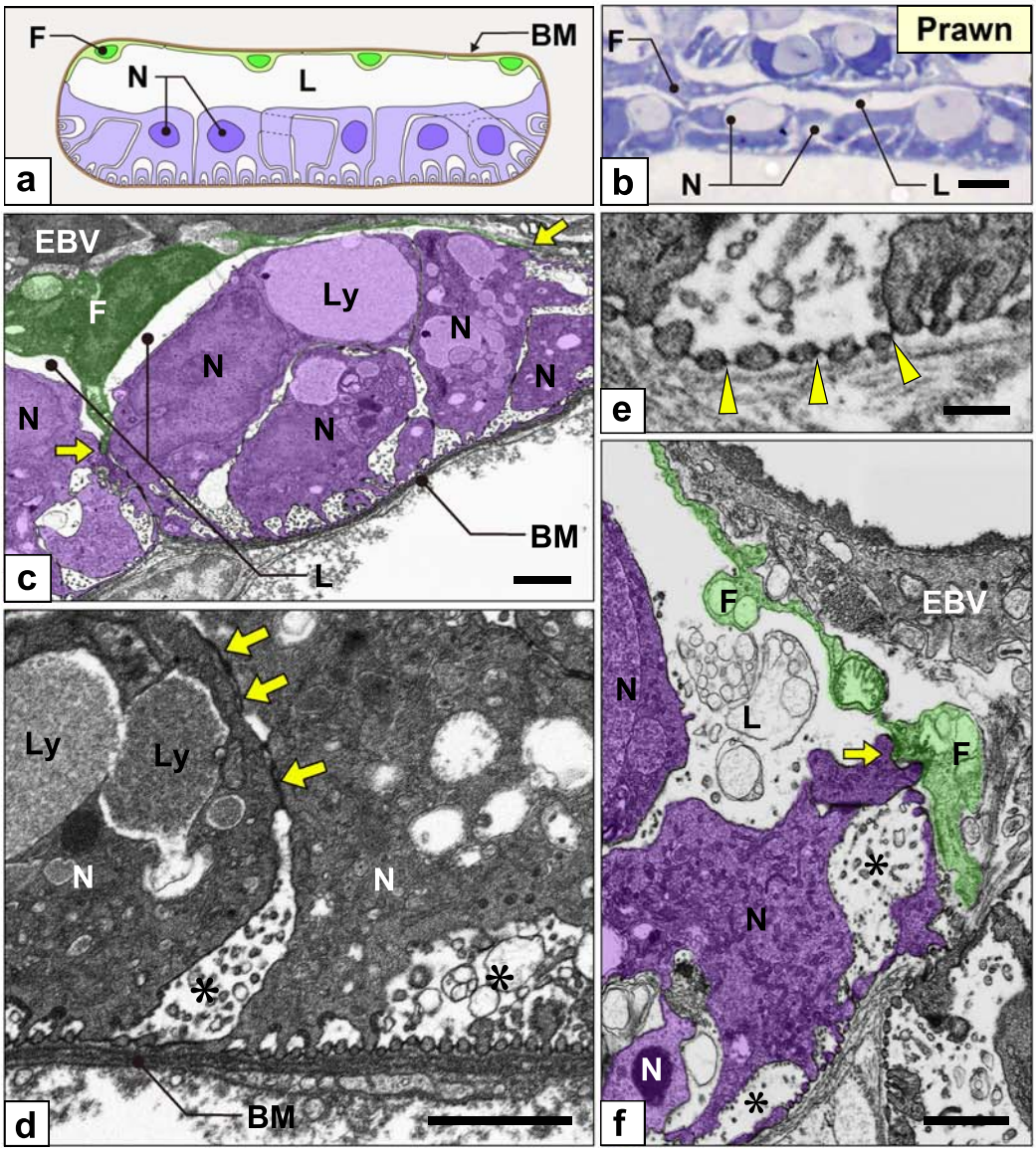

Figure 10
Miyaki et al.

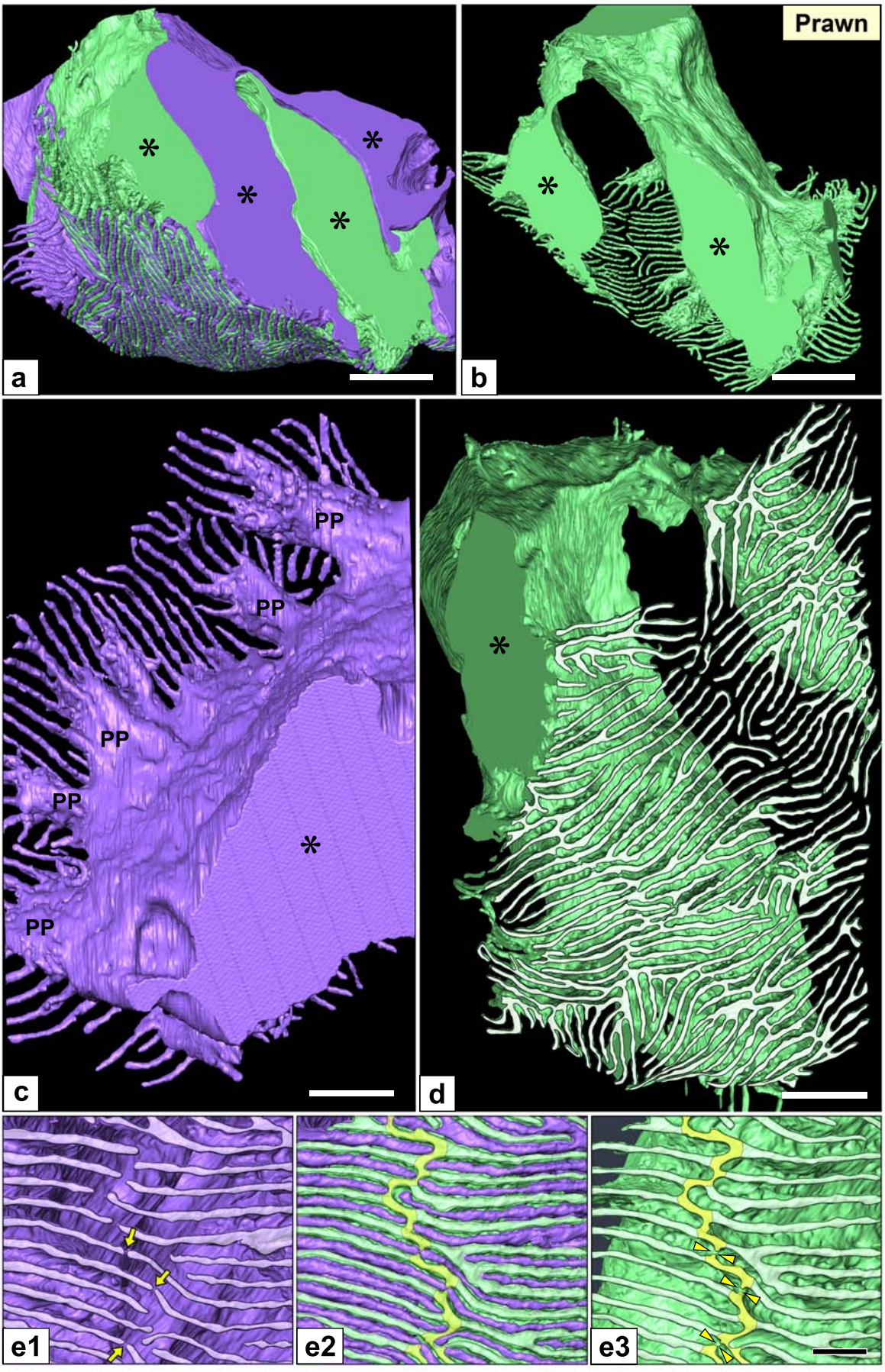

Figure 11
Miyaki et al.